Chapter 22

Treatment of Uncertainties in Radiation Dosimetry

Michael G. Mitch, Ph.D.[1], Larry A. DeWerd, Ph.D.[2], Ronaldo Minniti, Ph.D.[1], and Jeffrey F. Williamson, Ph.D.[3]

[1]Physics Laboratory, National Institute of Standards and Technology, Gaithersburg, Maryland

[2]Department of Medical Physics, University of Wisconsin-Madison, Madison, Wisconsin

[3]Department of Radiation Oncology, Virginia Commonwealth University, Richmond, Virginia

1. Methods for Classifying and Evaluating Uncertainties

1.1 Introduction

When one performs a physical measurement or a Monte Carlo simulation and obtains a numerical result, the following questions may be asked. How accurate is the result? Is the measurement or simulation method of high quality? Can the result be meaningfully compared with those of other laboratories, including primary standards laboratories? To answer these questions, it is necessary to assign an uncertainty to the result of the measurement or calculation. The uncertainty represents how confident the investigator is that the result is indicative of the "true" value of the quantity he is attempting to determine. Performing a rigorous uncertainty analysis is a critical element of the science of metrology, as it provides not only a means of assessing the quality of a measurement or calculation, but allows a quantitative comparison of results to be made. In the sections that follow, the methods for determining uncertainties will be discussed, along with how these methods are applied to the calculation of uncertainties in dosimetry measurements and calculations, from primary standards to clinical practice.

1.2 Classification of Uncertainties into Type A and Type B

There are two ways of classifying uncertainties, depending upon the methods used to determine them. "Type A" uncertainties are those that are calculated by statistical methods, and "Type B" uncertainties are evaluated by other means. This methodology was first recommended in 1981 by the Comité International des Poids et Mesures (CIPM) (Giacomo 1981), and included methods for combining the various components of uncertainty. An International Organization for Standardization (ISO) working group subsequently expanded the CIPM recommendations into the *Guide to the Expression of Uncertainty in Measurement* (GUM) (ISO 1993). In 1994, Technical Note 1297 was published by the National Institute of Standards and Technology (NIST), which summarized the ISO GUM (Taylor and Kuyatt 1994). The Type A component of uncertainty, u_A, can be calculated as s, the standard deviation of the mean of a series of measurements,

$$s = \left[\frac{1}{n(n-1)} \sum_{i=1}^{n} (z_i - \overline{z})^2 \right]^{1/2}, \tag{22.1}$$

where n is the number of measurements, z_i is the result of an individual measurement, and $\overline{z}$ is the mean,

$$\overline{z} = \frac{1}{n} \sum_{i=1}^{n} z_i. \tag{22.2}$$

A Type B component of uncertainty, u_B, is typically evaluated based on an instrument manufacturer's specifications, observed variations in previously acquired data, or the investigator's own knowledge and experience (scientific judgment). If no information is available to justify the choice of a particular probability distribution (i.e., normal), then it is reasonable to estimate the upper and lower limits, a_+ and a_-, respectively, for the value of a measured quantity, and use a uniform (rectangular) distribution to calculate u_B,

$$u_B = \frac{a_+ - a_-}{2\sqrt{3}}.$$ (22.3)

It should be noted that Type A and Type B uncertainties are not the same as "random" and "systematic" uncertainties. Random uncertainties vary for each measurement, yielding an observable "spread" in the data that will average to the conventional true value. Therefore, for a large number of measurements, theoretically there would be no uncertainty in the average value of the measured quantity. Systematic uncertainties are constant for each measurement, equal to the bias of the measurement technique, and are not observable in the data since the true value of the quantity being measured is unknown. Type A and Type B uncertainties involve analysis by the scientist. For example, measurements taken with an ion chamber would yield a mean and a standard deviation, which when expressed as a percent is a Type A uncertainty at $k = 1$. A Type B uncertainty is generally an estimate based upon scientific judgment. It may involve information given by the manufacturer. For example, if a device is stated by the manufacturer to have a total variation between the limits of $\pm L$, it is expected that 99% of the values would fall in this region. The Type B uncertainty would then be calculated from this probability distribution by $u_B\left(k = 1\right) = \frac{L}{\sqrt{3}}$.

1.3 Evaluation of Combined Standard Uncertainty and Expanded Uncertainty

The final reported quantity y from a measurement or calculation is often a function of several variables, x_i, each with its own Type A and Type B components of uncertainty,

$$y = f(x_1, x_2, ..., x_N).$$ (22.4)

Once all possible sources of uncertainty in a measurement or simulation are accounted for, assigned to Type A or Type B, and values of u_A and u_B are calculated, the uncertainty components are put together to form the combined standard uncertainty, u_C using the law of propagation of uncertainty

$$u_C = \left[\sum_{i=1}^{N}\left(\frac{\partial f}{\partial x_i}\right)^2 u^2(x_i) + 2\sum_{i=1}^{N-1}\sum_{j=i+1}^{N}\frac{\partial f}{\partial x_i}\frac{\partial f}{\partial x_j}u(x_i, x_j)\right]^{1/2}.$$ (22.5)

Note that equation (22.5) is derived from a first-order Taylor series approximation of the function f (Taylor and Kuyatt 1994), and that each value of $u(x_i)$ represents both the Type A and Type B components of uncertainty, calculated as

$$u^2(x_i) = u_A^2(x_i) + u_B^2(x_i). \qquad (22.6)$$

The second term of equation (22.5) contains the covariance $u(x_i, x_j)$, where

$$u(x_i, x_j) = \frac{1}{n-1} \sum_{k=1}^{n} (x_{ik} - \bar{x}_i)(x_{jk} - \bar{x}_j). \qquad (22.7)$$

The covariance will be non-zero if the variables x_i and x_j are correlated. It is often assumed that all variables x_i are independent, and the covariance is set to zero. (A case where the covariance is non-zero will be discussed in section 2.3.1.) If $u(x_i, x_j) = 0$, then equation (22.5) reduces to the familiar "square root of the sum-of-the-squares" method for combining the Type A and Type B components, yielding the combined standard uncertainty,

$$u_C = \left[\sum_{i=1}^{N} \left(\frac{\partial f}{\partial x_i} \right)^2 u^2(x_i) \right]^{1/2}. \qquad (22.8)$$

For example, if $y = x_1 x_2$,

$$u_C = \left[x_2^2 u_A^2(x_1) + x_2^2 u_B^2(x_1) + x_1^2 u_A^2(x_2) + x_1^2 u_B^2(x_2) \right]^{1/2}. \qquad (22.9)$$

Squaring both sides of the equation and dividing by y^2 yields

$$\left(\frac{u_C}{y} \right)^2 = \left(\frac{u_A(x_1)}{x_1} \right)^2 + \left(\frac{u_B(x_1)}{x_1} \right)^2 + \left(\frac{u_A(x_2)}{x_2} \right)^2 + \left(\frac{u_B(x_2)}{x_2} \right)^2, \qquad (22.10)$$

or expressed in terms of percentages,

$$\%u_C^2 = \%u_A^2(x_1) + \%u_B^2(x_1) + \%u_A^2(x_2) + \%u_B^2(x_2). \qquad (22.11)$$

Equations (22.10) and (22.11) are also true for $y = x_1 x_2^{-1}$. For $y = x_1 + x_2$ or $y = x_1 - x_2$,

$$u_C = \left[u_A^2(x_1) + u_B^2(x_1) + u_A^2(x_2) + u_B^2(x_2) \right]^{1/2}. \qquad (22.12)$$

If the probability distribution of the final measured or calculated result y is approximately normal, then the true value of the quantity is believed to lie within the interval

$y \pm u_C$ with a 67% level of confidence. The combined standard uncertainty is typically reported with measurement results from basic research, but in situations where the measurement result will be used where health and safety are a concern (such as in the field of medical physics), an expanded uncertainty is used. (Note that the conventional symbol for the expanded uncertainty, U, is not used here since it also represents the units of air-kerma strength.) The expanded uncertainty, V, is calculated using the formula

$$V = ku_C , \tag{22.13}$$

where k is the coverage factor. An expanded uncertainty with a coverage factor of 2 ($k = 2$) corresponds to an interval with a 95% level of confidence. Note that if the number of measurements is small (few degrees of freedom), the value of k used to relate the uncertainty to a level of confidence should be obtained from the t-distribution.

A list of all components of uncertainty, the combined standard uncertainty, and the expanded uncertainty is typically presented in tabular form, and is called the uncertainty budget for the measurement or calculation. When evaluating the quality of a measurement result, one should examine the uncertainty budget to determine how thoroughly the investigator has taken account of various components of uncertainty. A measurement with a reported low uncertainty may not necessarily be one of high quality if the reason for the low value is that some uncertainty components have been ignored. Also, a measurement result with high precision (low Type A uncertainty component) may not have high accuracy if the Type B uncertainties are not properly accounted for—the true value may actually fall outside the uncertainty interval. Making meaningful comparisons between the results of measurements from multiple laboratories is not possible without careful consideration and accounting of all components of uncertainty.

2. Uncertainties in Dosimetric Primary Standards

2.1 Introduction

National standards laboratories are charged with maintaining and disseminating primary standards for fundamental dosimetric quantities with the highest possible accuracy. This implies that the uncertainties of primary measurement results must be kept as low as possible, but at the same time, all possible sources of uncertainty must be accounted for in a detailed uncertainty budget. The magnitude of the uncertainty associated with measurements performed by standards laboratories defines the lower limit for achievable uncertainty in clinical measurements. In the sections that follow, NIST primary standards for medical dosimetry will be used as examples to illustrate the concept of an uncertainty budget and how uncertainties vary depending on the type of measurement being performed.

2.2 Brachytherapy

2.2.1 NIST Wide-Angle Free-Air Chamber (WAFAC)

The U.S. primary standard for directly realizing the air-kerma strength of low-energy, x-ray emitting ^{125}I, ^{103}Pd, and ^{131}Cs brachytherapy sources is the NIST Wide-Angle Free-Air Chamber (WAFAC), described in detail in chapter 16. The equation for calculating air-kerma strength, S_K, from WAFAC ionization current measurements is

$$S_K = \dot{K}_{air}(Q)d^2 = \left(\frac{\bar{W}}{e}\right)\left(\frac{d^2}{\rho_{air}V_{eff}}\right)K_{dr}(\dot{K})M_{det}(\dot{K},Q)\prod_i K_i \prod_j K_j(Q), \qquad (22.14)$$

where $\dot{K}_{air}(Q)$ is the air-kerma rate at a distance d, measured from the source to the aperture, $\bar{W}$ is the mean energy per ion pair expended when the initial kinetic energy of a charged particle is completely dissipated in air, e is the elementary charge, ρ_{air} is the density of air, V_{eff} is the effective chamber volume, $M_{det}(\dot{K},Q)$ is the net current (corrected for radioactive decay), and K_i are the correction factors. Each of the terms in this equation has an uncertainty associated with it, shown in table 22-1 for an ^{125}I source measurement. The lower limit (Type B components only) on the expanded uncertainty for ^{125}I source S_K measurements is 1.52% ($k = 2$). The value of s (Type A component) will vary, depending on the strength of the source. As an example, for an ^{125}I source with $S_K = 1$ U, a typical value of s is 0.85% ($k = 1$), yielding an expanded uncertainty of 2.28% ($k = 2$).

2.2.2 NIST Cavity Chambers

The U.S. primary standard for directly realizing the air-kerma strength of high-energy, gamma-ray–emitting brachytherapy sources is based on spherical, graphite-walled cavity ionization chambers, described in detail in chapter 16. For low dose-rate (LDR) ^{137}Cs sources, two separate steps are required to calibrate an unknown source, each with their own uncertainties. The first step involves calibrating several "working standard" sources in terms of air-kerma strength using a 1 cm^3 graphite cavity chamber. The uncertainty associated with this measurement is 0.63% ($k = 1$). The second step, employed on a routine basis for source calibration, involves measurement of the response of a 2.8 L spherical aluminum cavity chamber with the working standard source and the unknown source. This step involves two identical measurements, each with its own uncertainty of 0.41% ($k = 1$). Combining these three components using equation (22.11) yields a combined standard uncertainty of $u_C = 0.85\%$ ($k = 1$), or an expanded uncertainty of 1.70% ($k = 2$).

The calibration of LDR ^{192}Ir sources involves a three-step process. In the first step, a 50 cm^3 graphite cavity chamber is used to measure the air-kerma strength of a 50-source array. The uncertainty associated with this measurement is 0.53% ($k = 1$). The second step involves determining the calibration coefficient (air-kerma

Table 22-1. Uncertainty Budget for WAFAC Measurement of ^{125}I Brachytherapy Sources (Seltzer et al. 2003)

	Value	Type A (%)	Type B (%)
Net current, $M_{det}(\dot{K},Q)$	--	s	0.06
$\bar{W}/e$	33.97 J / C	--	0.15
Air density, ρ_{air}	1.196 mg / cm^3	--	0.03
Aperture distance, d	--	--	0.24
Effective chamber volume, V_{eff}	--	0.11	0.01
Decay correction, K_1	$T_{1/2} = 59.43\ d$	--	0.02
Recombination, $K_{dr}(\dot{K})$	<1.004	--	0.05
Attenuation in filter, $K_3(Q)$	1.0295	--	0.61
Air attenuation in WAFAC, $K_4(Q)$	1.0042	--	0.08
Source-aperture attenuation, $K_5(Q)$	1.0125	--	0.24
Inverse-square correction, K_6	1.0089	--	0.01
Humidity, $K_7(Q)$	0.9982	--	0.07
In-chamber photon scatter, $K_8(Q)$	0.9966	--	0.07
Source-holder scatter, K_9	0.9985	--	0.05
Electron loss, K_{10}	1.0	--	0.05
Aperture penetration, $K_{11}(Q)$	0.9999	--	0.02
External photon scatter, $K_{12}(Q)$	1.0	--	0.17
Combined standard uncertainty, u_C	$(s^2 + 0.762^2)^{1/2}$		
Expanded uncertainty, $V\ (k=2)$	$2(s^2 + 0.762^2)^{1/2}$		

strength per unit chamber current) of a 3.4 L spherical aluminum re-entrant chamber that is used for routine source calibrations. The re-entrant chamber current measurements have an uncertainty of 0.20% ($k = 1$). The third step is calibration of an unknown source in the re-entrant chamber, contributing an additional uncertainty of 0.37% ($k = 1$). Combining these three components using equation (22.11) yields a combined standard uncertainty of $u_C = 0.68\%$, or an expanded uncertainty of 1.36% ($k = 2$).

2.2.3 High Dose-Rate ^{192}Ir Source Calibrations

In the United States, air-kerma strength calibrations of high-dose rate (HDR) ^{192}Ir sources are currently performed by three Accredited Dosimetry Calibration Laboratories (ADCLs) using an interpolative method originally developed by Goetsch (Goetsch et al. 1991). The recently re-evaluated expanded uncertainty of this method is 2.15% ($k = 2$) (Stump et al. 2002). The use of Monte Carlo calculations

to generate the correction factors needed for a direct measurement method has been employed by the National Physical Laboratory (NPL), resulting in a substantially lower expanded uncertainty of 0.8% ($k = 2$) (Sander and Nutbrown 2006).

2.2.4 Beta-Particle–Emitting Source Calibrations

In contrast to air-kerma strength for photon sources, beta-particle source calibrations are based on the realization of absorbed dose to water using extrapolation ionization chambers. In the United States, the NIST medical extrapolation chamber is used to calibrate planar sources of ^{90}Sr or [106]Ru, as well as seed and line sources containing [90]Sr (Soares 2004). The expanded uncertainty of planar source absorbed dose measurements is 7% ($k = 2$), whereas that for seed and line sources is 10% ($k = 2$). The larger uncertainty in the seed and line source measurements is due to the greater difficulty associated with determining the area of the smaller (1 mm vs. 4 mm diameter) collection electrode. A multi-electrode extrapolation chamber developed by the Physikalisch-Technische Bundesanstalt (PTB), designed to achieve high spatial resolution and low measurement uncertainty, is capable of measuring absorbed dose to water at 2 mm depth with a maximum expanded uncertainty of 6.0% ($k = 2$) (Bambynek 2002). A similar instrument to that at NIST is used by the Nederlands Meetinstitut (NMi) to calibrate planar sources with an expanded uncertainty of 11% ($k = 2$) (van der Marel and Van Dijk 2003).

2.3 External Beam

2.3.1 NIST Cavity Chambers for [60]Co Air-Kerma Calibrations

Air-kerma calibrations of therapy-level ^{60}Co beams at NIST are performed using two spherical, graphite-walled cavity ionization chambers with volumes of 1 cm³ and 10 cm³ (Minniti et al. 2006). The final value of the air-kerma rate is determined by taking the mean value of the air-kema rates from each chamber. In this case, combining the uncertainties from each chamber is not straightforward, since the Type B components are correlated and the second term in equation (22.5) is not zero.

To illustrate this we will first review the measurement of the air kerma rate performed with the two graphite-wall air-ionization chambers. The air kerma rate, $\dot{K}_{air}(Q)$, is determined from each one of the ionization chamber's current measurement $M_{det}(\dot{K},Q)$ as

$$\dot{K}_{air}(Q) = \left(\frac{\bar{W}}{e}\right)\left(\frac{1}{\rho_{air}V}\right)\left(\frac{1}{1-\bar{g}}\right)\frac{(\bar{\mu}_{en}/\rho)_{air}}{(\bar{\mu}_{en}/\rho)_{gr}}\frac{(\bar{L}_{\Delta}/\rho)_{gr}}{(\bar{L}_{\Delta}/\rho)_{air}} \quad (22.15)$$
$$K_{dr}(\dot{K})M_{det}(\dot{K},Q)K_{stem}K_{wall}(Q)K_{h}(Q),$$

where V is the volume of air inside the chamber cavity, ρ_{air} is the density of dry air at the measurement temperature and pressure, $\overline{W}/e$ is the mean energy expended in dry air by electrons per ion pair formed (33.97 J/C), and $\overline{g}$ is the mean fraction of the initial kinetic energy of secondary electrons liberated by photons that is lost through radiative processes in air and is equal to 0.0032 for ^{60}Co (Seltzer and Bergstrom 2003). Other terms in equation (22.15) include the ratio of the mean Spencer-Attix electron-fluence-weighted electron mass stopping powers for graphite and air, $\overline{L}_{\Delta}/\rho$, and the ratio of the mean photon-energy–fluence-weighted mass energy-absorption coefficients for air and graphite, $\overline{\mu}_{en}/\rho$. The correction factors in equation (22.15) are discussed elsewhere (Seltzer and Bergstrom 2003), and include: $K_h(Q)$, a humidity correction for the effects of moist air; $K_{dr}(\dot{K})$ a correction for the loss of ionization due to ion recombination; K_{stem}, a correction for stem scattering; and $K_{wall}(Q)$, the correction for wall absorption and scattering.

The air-kerma rate at a distance of 1 m from the source is determined from measurements made with each of the two small volume primary-standard ionization chambers as

$$\overline{\dot{K}} = \frac{\dot{K}_1 + \dot{K}_{10}}{2},\tag{22.16}$$

where $\overline{\dot{K}}$ is the mean value, and $\dot{K}_1$ and $\dot{K}_{10}$ represent the air-kerma rates determined using the chambers with volumes of 1 cm^3 and 10 cm^3, respectively. For each of the quantities $\dot{K}_1$, $\dot{K}_{10}$, and $\overline{\dot{K}}$, the relative combined standard uncertainties are denoted here by $\dfrac{u_C\left(\dot{K}_1\right)}{\dot{K}_1}$, $\dfrac{u_C\left(\dot{K}_{10}\right)}{\dot{K}_{10}}$ and $\dfrac{u_C\left(\overline{\dot{K}}\right)}{\overline{\dot{K}}}$, respectively. Table 22-2 provides a summary of the uncertainty analysis (also referred to as an uncertainty budget as discussed in the introductory section of this chapter) for this primary-standard measurement of the air-kerma rate. The uncertainty components listed in table 22-2 are the relative standard uncertainties (or uncertainty components) for each of the parameters and corrections that appear in equation (22.15). They are grouped, for a given chamber, in two columns according to the type of evaluation that was used for the uncertainties, i.e., Type A and Type B.

The relative combined standard uncertainties shown in table 22-2 for each chamber are obtained from the quadratic sum as

$$\left(\frac{u_C\left(\dot{K}_s\right)}{\dot{K}_s}\right)^2 = \left(\frac{u_A\left(\dot{K}_s\right)}{\dot{K}_s}\right)^2 + \left(\frac{u_B\left(\dot{K}_s\right)}{\dot{K}_s}\right)^2,\tag{22.17}$$

Table 22-2. Uncertainty Budget for the Primary Standard Measurement of Air-Kerma Rate

Uncertainty Components	$\dot{K}_1$		$\dot{K}_{10}$	
	Type A (%)	Type B (%)	Type A (%)	Type B (%)
Charge	0.10	0.10	0.06	0.10
Time	--	0.05		0.05
Volume	0.10	0.10	0.16	0.10
Air-density correction (temperature and pressure)	--	0.03	--	0.03
Distance (axial)	--	0.02	--	0.02
$K_{dr}(\dot{K})$, loss of ionization due to recombination	0.01	0.05	0.05	0.10
K_{stem}, stem scatter	--	0.05	--	0.05
Axial nonuniformity	--	0.02	--	0.05
Radial nonuniformity	--	0.01	--	0.01
Density of dry air at $T = 0\ °C$ and $p = 1$ atm	--	0.02	--	0.02
$K_h(Q)$, humidity correction	--	0.06	--	0.06
$K_{wall}(Q)$, wall correction	--	0.17	--	0.17
Ratio of mean photon energy-absorption coefficients, air/graphite	--	0.04	--	0.04
Product of $\bar{W}/e$ and ratio of mean electron mass electronic stopping powers, graphite/air	--	0.11	--	0.11
$(1-\bar{g})$, radiative-loss correction	--	0.03	--	0.03
Quadratic sums	0.14	0.28	0.18	0.29
Relative combined standard uncertainties of $\dot{K}_1$ and $\dot{K}_{10}$	0.31		0.34	
Relative combined standard uncertainty of $\bar{\dot{K}}$	0.31			
Relative expanded ($k = 2$) uncertainty of $\bar{\dot{K}}$	0.62			

where the subscript "s" denotes the nominal volume of 1 and 10 (expressed in units

of cm^3) for the two chambers. Note in table 22-2 that the values of $\left(\dfrac{u_A\left(\dot{K}_s\right)}{\dot{K}_s}\right)$ and

$\left(\dfrac{u_B\left(\dot{K}_s\right)}{\dot{K}_s}\right)$ are obtained for a given chamber by performing the square root of the

sum of squares of all the uncertainty components listed for a given chamber using
equation (22.11). As mentioned previously, in relation to equation (22.7), this
assumes that each of the components listed in table 22-2 for a given chamber are
independent. That is, for example, the measurement of charge and the measurement
of volume are completely independent for a given chamber. As a result, and as shown
in table 22-2, the values obtained for the relative combined standard uncertain-

ties $\dfrac{u_C\left(\dot{K}_1\right)}{\dot{K}_1}$, and $\dfrac{u_C\left(\dot{K}_{10}\right)}{\dot{K}_{10}}$, for each chamber are 0.31% and 0.34%, respectively.

Up to this point we have obtained the uncertainty of the measurement of the air-
kerma rate made with each chamber. To calculate the uncertainty of the final value
of air-kerma rate determined from equation (22.15), one must combine the relative

combined standard uncertainties $\dfrac{u_C\left(\dot{K}_1\right)}{\dot{K}_1}$ and $\dfrac{u_C\left(\dot{K}_{10}\right)}{\dot{K}_{10}}$ for each chamber. In doing

this, however, we must account for possible correlations between the measurements
made with the two chambers. For this we will introduce the correlation coefficient,
$r(x_i,x_j)$, which is a parameter that is used to estimate the degree of correlation
between two variables x_i and x_j. Such variables are the ones that appear listed
in table 22-2. The correlation coefficient $r(x_i,x_j)$ between any of the variables listed in
table 22-2 can be expressed in terms of the covariance $u(x_i,x_j)$, defined by equation
(22.7), as

$$r(x_i,x_j)=\frac{u(x_i,x_j)}{u(x_i)u(x_j)}.\qquad(22.18)$$

If the variables x_i and x_j are completely independent, then $r(x_i,x_j)=0$. For exam-
ple, the measurement of the charge and the volume are completely independent and
therefore there is no correlation. However, if a variable is measured using the same
method, the correlation $r(x_i,x_j)$ can have a non-zero value. To illustrate this,
consider the first parameter in table 22-2, the measurement of charge. The compo-
nents listed under Type B have to do with any type of uncertainty related to the
charge that is nonstatistical in nature, such as uncertainty in the method used or the
uncertainty in the calibration of the instrument used to measure the charge.
Although the charge is being measured with two different chambers, the method for
collecting the charge as well as the electrometer used are the same. As a result, the

charge measurements made with both chambers are correlated to some degree. This implies that the correlation coefficient can have a non-zero value for this case between zero and unity. Another example is if one considers any of the calculated corrections that are applied to the measurement of air-kerma rate that are listed in table 22-2. These calculated corrections are obtained using exactly the same method and using the same Monte Carlo codes. Therefore, it is reasonable to assume that there will be a high degree of correlation between the Type B uncertainties for these calculated corrections. The approach followed is to assign a value to the correlation coefficient $r(x_i, x_j)$ between each pair of components listed in table 22-2 to take into account the degree of correlation. For this analysis, all Type A uncertainty components of the two chambers are assumed to be completely uncorrelated ($r(x_i, x_j) = 0$), while the Type B uncertainty components are assumed to be completely correlated ($r(x_i, x_j) = 1$).

The values of $r(x_i, x_j)$ can then be used to evaluate equation (22.5), which can be written in terms of the correlation coefficient as

$$u_C = \left[\sum_{i=1}^{N} \left(\frac{\partial f}{\partial x_i} \right)^2 u^2(x_i) + 2 \sum_{i=1}^{N-1} \sum_{j=i+1}^{N} \frac{\partial f}{\partial x_i} \frac{\partial f}{\partial x_j} u(x_i) u(x_j) r(x_i, x_j) \right]^{1/2}. \quad (22.19)$$

Equation (22.19) is derived by substituting equation (22.18) into equation (22.5). This evaluation results in a relative combined standard uncertainty for the air-kerma rate, $\dfrac{u_C(\bar{\dot{K}})}{\bar{\dot{K}}} = 0.31\%$.

To illustrate this in a simpler way, instead of evaluating equation (22.19) for all of the components listed in table 22-2, we will combine each one of the four relative combined standard uncertainties given at the end of the uncertainty budget shown in table 22-2 for each chamber, $\left(\dfrac{u_A(\dot{K}_1)}{\dot{K}_1} \right)$, $\left(\dfrac{u_B(\dot{K}_1)}{\dot{K}_1} \right)$, $\left(\dfrac{u_A(\dot{K}_{10})}{\dot{K}_{10}} \right)$, and $\left(\dfrac{u_A(\dot{K}_1)}{\dot{K}_1} \right)$. We will consider that the Type A uncertainties are uncorrelated ($r(x_i, x_j) = 0$) and that Type B uncertainties are completely correlated ($r(x_i, x_j) = 1$). This approach will provide an upper bound for the relative combined uncertainty of the mean air-kerma rate. With these assumptions, the relative combined standard uncertainty of the mean value for the air-kerma rate, $\dfrac{u_C(\bar{\dot{K}})}{\bar{\dot{K}}}$, can be derived from equations (22.4) and (22.19), considering $\bar{\dot{K}} = y = \dfrac{1}{2}(x_1 + x_2)$, where $x_1 = \dot{K}_1$ and $x_2 = \dot{K}_{10}$,

$$u_C = \left[\begin{array}{l} \left(\frac{1}{2}\right)^2 u_A^2(\dot{K}_1) + \left(\frac{1}{2}\right)^2 u_B^2(\dot{K}_1) + \left(\frac{1}{2}\right)^2 u_A^2(\dot{K}_{10}) + \left(\frac{1}{2}\right)^2 u_B^2(\dot{K}_{10}) \\ + 2\left(\frac{1}{2}\right)\left(\frac{1}{2}\right) u_B(\dot{K}_1) u_B(\dot{K}_{10}) \end{array} \right]^{1/2} . \qquad (22.20)$$

Simplifying yields

$$u_C = \frac{1}{2} \left\{ u_A^2(\dot{K}_1) + u_A^2(\dot{K}_{10}) + \left[u_B(\dot{K}_1) + u_B(\dot{K}_{10}) \right]^2 \right\}^{1/2} . \qquad (22.21)$$

Noting that $\bar{\bar{K}} \approx \dot{K}_1 \approx \dot{K}_{10}$ (Minniti et al. 2006), this results in the following expression

$$\frac{u_C(\bar{\bar{K}})}{\bar{\dot{K}}} \approx \frac{1}{2} \left\{ \left(\frac{u_A(\dot{K}_1)}{\dot{K}_1} \right)^2 + \left(\frac{u_A(\dot{K}_{10})}{\dot{K}_{10}} \right)^2 + \left(\frac{u_B(\dot{K}_1)}{\dot{K}_1} + \frac{u_B(\dot{K}_{10})}{\dot{K}_{10}} \right)^2 \right\}^{1/2} . \qquad (22.22)$$

The evaluation of equation (22.22) results in a value of $\dfrac{u_C(\bar{\bar{K}})}{\bar{\dot{K}}} = 0.31\%$. The relative expanded uncertainty of the air-kerma rate $\bar{\dot{K}}$ is obtained by multiplying the relative combined standard uncertainty by a coverage factor of 2, giving 0.62%. The complete uncertainty analysis is summarized in table 22-2.

We would like to point out an interesting observation which can be clearly seen for the particular case when the uncertainty components in equation (22.22) are similar in value, i.e., $\left(\dfrac{u_A(\dot{K}_1)}{\dot{K}_1} \right) \approx \left(\dfrac{u_A(\dot{K}_{10})}{\dot{K}_{10}} \right)$ and $\left(\dfrac{u_B(\dot{K}_1)}{\dot{K}_1} \right) \approx \left(\dfrac{u_B(\dot{K}_{10})}{\dot{K}_{10}} \right)$. For this particular case, equation (22.22) can be reduced to the following expression (or the corresponding one in terms of K_1)

$$\frac{u_c(\bar{\bar{K}})}{\bar{\dot{K}}} \approx \left\{ \frac{1}{2} \left(\frac{u_A(\dot{K}_{10})}{\dot{K}_{10}} \right)^2 + \left(\frac{u_B(\dot{K}_{10})}{\dot{K}_{10}} \right)^2 \right\}^{1/2} . \qquad (22.23)$$

As described above, the first term results from combining the Type A uncertainties, which were assumed to be uncorrelated, while the second term results from combining the Type B uncertainties, which were assumed to be completely correlated. Note the number 2 in the denominator of the first term. This happens to be the number of chambers used. Therefore, if more chambers would have been used, this term would become smaller for an increasing number of chambers. However,

the second term would have a finite, non-zero value independent of the number of chambers.

2.3.2 NIST Water Calorimeter for ^{60}Co Absorbed-Dose-To-Water Calibrations

The NIST primary standard instrument for measuring absorbed dose to water is the Domen water calorimeter (Domen 1994). The water calorimeter is used to measure the temperature rise due to the absorbed radiation in water. The temperature rise is related to the absorbed dose in water, D_w, as

$$D_w = c\Delta T \frac{1}{1-K_{HD}} \prod_i K_i, \qquad (22.24)$$

where c is the specific heat capacity of water at the calorimeter operating temperature, ΔT is the temperature rise, and K_{HD} is the heat defect due to radiation-induced chemical changes in the water, resulting in a correction applied to the measurement equal to $\dfrac{1}{1-K_{HD}}$. Other corrections in equation (22.24), K_i, account for the beam attenuation from the calorimeter lid and glass vessel wall. The temperature change is measured by a pair of thermistors mounted within a glass container filled with high-purity water.

The measurement of the absorbed dose rate to water using the NIST water calorimeter is performed at a distance of 1 m from the source. That is, the detection point defined by the location of the thermistor probe defines the source-to-detector distance. The detection point is located at a depth of 5 cm below the water surface. The uncertainty associated with positioning the thermistor probe and the glass vessel to ensure these geometrical conditions contributes to the overall uncertainty of the primary measurement of the absorbed dose rate to water. In addition, each one of the terms that appear in equation (22.24) has an uncertainty and contributes as well to the overall uncertainty. Table 22-3 shows all the uncertainty components involved in the primary measurement of absorbed dose rate to water at NIST from a ^{60}Co gamma-ray beam. The source of each one of these uncertainties has been explained in detail in the original work by Domen (1994). An additional component of uncertainty has been added more recently and is listed in table 22-3 under "field size" (Minniti et al. 2007). This additional Type B uncertainty component was evaluated using a uniform distribution as described in equation (22.3). The relative combined standard uncertainty of the absorbed dose rate to water, $\dot{D}_w$, is obtained by calculating the square root of the sum of squares of all uncertainty components listed in table 22-3 by using equation (22.11). As shown in table 22-3, the relative combined standard uncertainty of the measurement of the absorbed dose rate to water is 0.42%, while the expanded uncertainty of the absorbed dose rate to water is 0.84% ($k = 2$).

Table 22-3. Uncertainty Analysis for the Primary Standard Measurement of the Absorbed-Dose-Rate-to-Water, $\dot{D}_w$ (Minniti et al. 2007)

Uncertainty Components	$\dot{D}_w$	
	Type A (%)	Type B (%)
Heat defect	--	0.30
Reproducibility of measurement groups	0.15	--
Beam attenuation from glass wall	--	0.10
Beam attenuation from calorimeter lid	0.05	--
Field size	--	0.23
Vessel positioning	--	0.02
Thermistor calibration	--	0.01
Water density	--	0.02
Quadratic sum	0.16	0.39
Relative combined standard uncertainty of the absorbed-dose-rate-to-water measurement at 5 cm in water	0.42	
Relative expanded ($k = 2$) uncertainty of the absorbed-dose-rate-to-water measurement at 5 cm in water	0.84	

2.3.3 NIST Free-Air Chambers for X-Ray Beam Calibrations

There are four free-air chambers at NIST that are used to realize the air-kerma rates from x-ray beams directly (O'Brien 2004). The Attix chamber (10 kV to 50 kV) and Lamperti chamber (10 kV to 60 kV) are used for mammography ionization chamber calibrations, while the Ritz chamber (20 kV to 100 kV) and Wyckoff-Attix chamber (50 kV to 300 kV) are used for superficial and orthovoltage x-ray calibrations. These free-air chambers constitute the primary standards for measuring the air-kerma rate from x-ray beams. In all cases, the appropriate free-air chamber is used to determine the air-kerma rate at a given distance from the x-ray source (typically around 1 m) and for a given x-ray beam quality. The calibrated x-ray beams are then used to determine the calibration coefficient (air-kerma rate per unit ionization current) of a reference-class cavity ionization chamber. For the Ritz and Wyckoff-Attix chambers, the relative combined standard uncertainty of the air-kerma rate measurement is 0.47% ($k = 1$). The uncertainty of the measurement of the ionization current made with the reference-class cavity chamber is 0.17% ($k = 1$). Combining the uncertainties of the reference air-kerma rate and the ionization current yields a combined standard uncertainty for the calibration coefficient of 0.50% ($k = 1$) and an expanded uncertainty of 1.00% ($k = 2$). For mammography beam calibrations, the combined standard uncertainty of the air-kerma rate

measurement using the Attix chamber is 0.42% ($k = 1$). The reference class cavity chamber ionization current measurement contributes 0.21% ($k = 1$), for a combined standard uncertainty on the calibration coefficient of 0.46% ($k = 1$) or an expanded uncertainty of 0.92% ($k = 2$). Note that in both cases the uncertainty of the cavity chamber calibration coefficient is dominated by that of the primary standard, an absolute measurement. The measurement of ionization current using a high-quality, stable reference-quality cavity chamber can be achieved with high precision and reproducibility, resulting in little loss of accuracy. Such reference cavity chambers are used to transfer primary standards to secondary calibration laboratories and ultimately to therapy clinics, which will be discussed in the next section.

3. Uncertainties in the Transfer of Standards

3.1 Introduction

Once a primary standard for a dosimetric quantity has been established at a national standards laboratory, a practical method for transferring that standard to radiation therapy clinics must be developed. This may be accomplished by having a national standards laboratory calibrate either a radioactive source or an instrument that is then sent to the clinic. In a large country such as the United States, this would create an unmanageable workload for the national standards laboratory. Therefore, standards are typically transferred through one or more secondary calibration laboratories that calibrate sources or instruments for clinics. Even though clinical measurements are then two steps removed from the primary standard, traceability to that primary standard is still achieved as long as there is an unbroken chain of measurements from the clinic to the national standards laboratory. Each subsequent measurement in this traceability chain will add uncertainty to the value of the dosimetric quantity, although the majority of the uncertainty is from the establishment of the primary standard. This smaller addition of uncertainty is caused by the fact that the high precision for a secondary standard will minimize the additional uncertainty added at each step from the national standards laboratory to the clinic. In the following sections, the U.S. system of secondary calibration laboratories for medical dosimetry will be described as an example of how primary standards are transferred to clinics.

3.2 Transfer of Dosimetry Standards to Secondary Calibration Laboratories

3.2.1 Source-based Transfer of the Air-Kerma Strength Standard

For low-energy, photon-emitting ^{125}I, [103]Pd, and [131]Cs brachytherapy sources, the primary NIST standard for air-kerma strength is transferred to three secondary calibration laboratories that are accredited by the American Association of Physicists in

Medicine (AAPM). These laboratories are known as Accredited Dosimetry Calibration Laboratories (ADCLs). The primary air-kerma strength standard is transferred by means of sending a batch of three NIST-calibrated sources of a given model to each ADCL in turn. The ADCLs measure the response (ionization current) of a well-ionization chamber to each source, and calculate the ratio of the air-kerma strength to the current, yielding the calibration coefficient for the well chamber. The uncertainties associated with the well chamber measurement are added [using the law of propagation of uncertainty, equation (22.5)] to that of the primary standard air-kerma strength value. Thus, NIST traceability resides in the calibration coefficient of an ADCL well chamber. It should be noted that source manufacturers send a total of five seeds to NIST for the initial calibration, two of which are returned to them for use in setting up their methodology for calibrating sources coming off the production line (figure 22-1). Unlike the ADCLs, whose measurement techniques must fulfill certain criteria specified by their AAPM accreditation (including a detailed uncertainty budget), each manufacturer may use whatever method it chooses to set up and maintain an in-house, traceable standard.

To maintain the accuracy of the ADCL secondary standard, the AAPM has published recommendations for annual circulation of an additional three-seed batch among NIST and the ADCLs (DeWerd et al. 2004). Upon receipt of the sources from the manufacturer, NIST calibrates them in terms of air-kerma strength, then characterizes the sources using several techniques. The x-ray spectrum emergent from the source is measured to ensure that there are no additional energies due to unexpected changes in source design, and that if fluorescent x-rays from source components are present, their intensity relative to that of the photons from the radionuclide decay is the same as that measured from previous sources calibrated by NIST. Radiochromic film contact exposure measurements are performed on
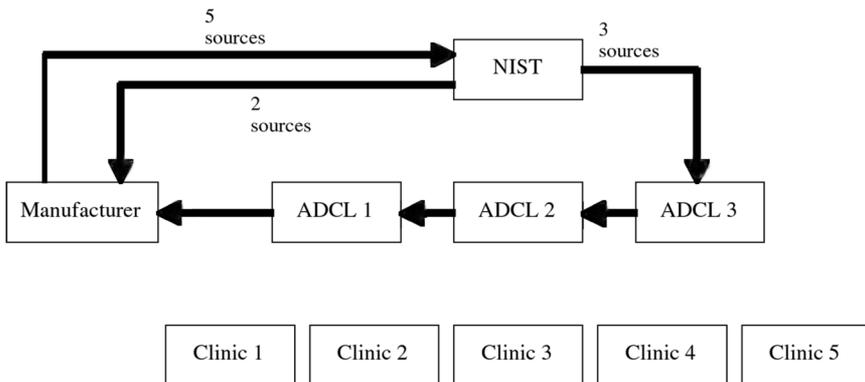

Figure 22-1. Transfer of NIST primary air-kerma-strength standard for brachytherapy sources to the ADCLs and manufacturer.

each source to verify consistency in the placement of internal source components. Anisotropy of emissions from the source is measured both around the long axis (WAFAC current measurements) and around an axis perpendicular to the long axis (x-ray spectrometry) of the source. Finally, the response of at least two different types of well chambers is measured, and a response coefficient, the quotient of well chamber current and air-kerma strength (reciprocal of the calibration coefficient) is calculated. The response coefficients for the three-seed batch are compared with those obtained in the past from sources of the same model. According to AAPM recommendations, if there is agreement within ±2.00% between the NIST response coefficients of the sources being measured and those obtained in the past, these sources will be circulated amongst the ADCLs. The ADCLs will make similar comparisons of their well chamber measurement results (calibration coefficients) between the current batch and the batch initially used to transfer the NIST standard. If NIST and all three ADCLs find agreement within a tolerance level of ±2.00%, then the standard is considered to be accurately maintained, and no changes are made. If measurement results are out of tolerance, the reason for the discrepancy is investigated. Because of the difference in the response of the WAFAC and well chambers due to energy dependence and measurement geometry effects, x-ray spectra and anisotropy measurements are often used to identify the causes of such discrepancies.

The NIST primary air-kerma strength standard for ^{137}Cs and LDR ^{192}Ir brachytherapy sources was transferred to the ADCLs through calibration of sources at NIST using the spherical-aluminum cavity chamber or the spherical-aluminum re-entrant chamber, respectively. Additional characterization measurements include x-ray spectrometry, well chamber response, and radiochromic film contact exposures. According to published AAPM recommendations, annual calibrations of sources or calibration instrumentation should be performed by NIST or an ADCL (Li et al. 2007). Since the sensitivity of well chamber calibration coefficients to small variations in source design is much lower for ^{137}Cs and ^{192}Ir sources than for ^{125}I, ^{103}Pd, and ^{131}Cs sources due to the higher energy of emissions of the former, annual circulation of multiple-source batches amongst NIST and the ADCLs is not necessary to maintain secondary standards accurately. This is demonstrated by the results of periodic NIST-directed Measurement Quality Assurance (MQA) tests of ADCL calibrations of both sources and well chambers.

3.2.2 Ionization-Chamber-based Transfer of Air-Kerma Strength Standard

The primary standards maintained at NIST for air kerma from x-ray, ^{137}Cs, and ^{60}Co gamma-ray beams as well as the primary standard for absorbed dose to water from ^{60}Co beams are transferred to secondary standard dosimetry facilities (SSDFs) throughout the country via the calibration of reference class ionization chambers owned by the SSDFs. The three AAPM ADCLs mentioned in the previous sections also form part of this network. Reference class ionization chambers owned by the SSDFs are sent to NIST to be calibrated. Such chambers are also referred to as

secondary standard chambers, indicating that they are used for transferring the primary measurement to a secondary facility.

A brief description of the chamber calibration process is described below with a special emphasis placed on the uncertainty analysis. To illustrate this, we will consider the calibration of a secondary standard chamber in a ^{60}Co gamma ray beam in terms of the quantity air-kerma rate. The illustration of the uncertainty analysis for this case is very similar to the calibration of a chamber in any of the other x-ray and gamma-ray beams in terms of air kerma rate or absorbed dose rate to water. During a calibration, the goal is to determine the calibration coefficient of an ionization chamber, N_K, given by

$$N_K = \frac{\dot{K}}{I}, \tag{22.25}$$

where $\dot{K}$ is the reference air-kerma rate determined at NIST using the primary standard instruments [as described in the section of this chapter dedicated to primary measurements, equation (22.14)]. I is the measured value of the ionization current with the secondary standard chamber being calibrated. The measured value of I includes corrections to account for ion-recombination effects and for deviations of the ambient temperature and pressure from the NIST reference conditions of 22 °C and 101.325 kPa (1 atm), respectively. The calibration coefficient is expressed in units of gray per coulomb.

Table 22-4 lists all the uncertainty components that contribute to the measurement of the ionization current, I. The relative combined standard uncertainty associated with the response of the ionization chamber (mainly given by the measurement of the ionization current and its corresponding corrections) is

$$\frac{u_C(I)}{I} = \sqrt{\sum_i \left(\frac{u_{Ai}(I)}{I}\right)^2 + \sum_j \left(\frac{u_{Bj}(I)}{I}\right)^2}, \tag{22.26}$$

where $u_{Ai}(I)$ and $u_{Bj}(I)$ represent the Type A and Type B uncertainty components, respectively. The relative combined standard uncertainty for the calibration coefficient, $\frac{u_C(N_K)}{N_K}$, is then

$$\frac{u_C(N_K)}{N_K} = \sqrt{\left(\frac{u_C(\dot{K})}{\dot{K}}\right)^2 + \left(\frac{u_C(I)}{I}\right)^2}. \tag{22.27}$$

The value for the relative combined standard uncertainty $\frac{u_C(N_K)}{N_K}$ is 0.36%.

The relative expanded uncertainty ($k = 2$) for the calibration coefficient measured at NIST, N_K is 0.72%. Similar uncertainty analyses for the absorbed-dose-to-water

Table 22-4. Uncertainty Analysis for the Calibration of the Secondary
Standard Ionization Chambers in Terms of Air-Kerma

Uncertainty Components	Type A (%)	Type B (%)
Charge	0.10	0.10
Time	--	0.05
Air density correction (temperature and pressure)	--	0.03
Distance	--	0.02
$K_{dr}(\dot{K})$, loss of ionization due to recombination	0.01	0.05
Probe orientation	--	0.01
$K_h(Q)$, humidity	--	0.06
^{60}Co decay[a]	--	0.01
Quadratic sum	0.10	0.14
Relative combined standard uncertainty of the chamber current I	0.17	
Relative combined standard uncertainty of $\bar{\dot{K}}$	0.31	
Relative combined standard uncertainty of the calibration coefficient, N_K	0.36	
Relative expanded ($k = 2$) uncertainty of the calibration coefficient, N_K	0.71 ($\rightarrow$ 0.8)	

[a] The air-kerma rate determined by the primary-standard instruments has been transferred to
the ^{60}Co source and is then decay-corrected to the time of the calibration measurement. For
this correction NIST uses a half-life of 1925.3 days with a standard uncertainty of 0.5 day.

calibration in ^{60}Co beams and for the air-kerma calibration in x-ray beams can be
found elsewhere (Minniti et al. 2007; Lamperti and O'Brien 2001).

3.3 Transfer of Dosimetry Standards from Secondary Calibration Laboratories to Clinics

Once NIST-traceable secondary standards have been established at each ADCL,
therapy clinics send their well- or reference-class cavity ionization chambers to one
of the ADCLs for calibration. For ^{60}Co air-kerma rate and absorbed dose as well as
x-ray beam air-kerma rate, ADCLs use their NIST-calibrated reference class ioniza-
tion chambers to calibrate their in-house ^{60}Co or x-ray beam, then substitute a
clinic's chamber in the beam to transfer the calibration. In the case of brachyther-
apy source calibrations, clinics send their well-ionization chamber to an ADCL or
sometimes have a brachytherapy source calibrated. For sources that contain long-
lived radionuclides (i.e., ^{137}Cs, ^{90}Sr), each ADCL will already have a NIST-
calibrated source on-site that can be used to calibrate the clinic's chamber. For
short-lived sources (i.e., ^{192}Ir, ^{125}I, ^{103}Pd, and ^{131}Cs), the ADCL will acquire a
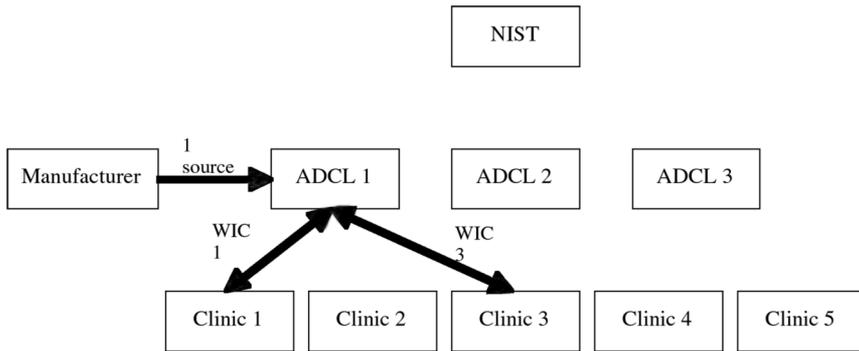
Figure 22-2. Calibration of clinical well-ionization chambers (WIC) by ADCL.

specific model source from the manufacturer, calibrate it using their well chamber with a NIST-traceable calibration coefficient, then transfer the calibration to the clinic's well chamber. This process is illustrated in figure 22-2, where ADCL 1 has acquired a brachytherapy source from the manufacturer to calibrate well chambers from Clinics 1 and 3.

The transfer of the calibration coefficient at the ADCLs adds uncertainty to the calibration coefficient provided to the user. The amount of the uncertainty added depends on the type of calibration and the details of the process. For example, where there is good signal to noise (ion chambers in a ^{60}Co beam), the additional uncertainty is lower than in the case of low-energy brachytherapy sources, where the leakage of the electrometer may be significant compared to the signal. Table 22-5 shows some representative values for the ADCL uncertainty compared to that of the primary standard.

Table 22-5. ADCL and NIST Uncertainties of Calibration Quantities at $k = 2$

Type of Calibration	ADCL Uncertainty (%)	NIST Uncertainty (%)
Cobalt air-kerma	1.5	1.4
Cobalt absorbed dose to water	1.4	1.2
Low-dose brachytherapy well chambers	2.4	1.9[a]
Low-dose brachytherapy seeds	1.9	1.4
High-dose brachytherapy well chambers	2.6	1.7[b]
X-ray air-kerma	1.0	0.8
Diagnostic air-kerma	1.9	0.8
Mammography air-kerma	1.9	0.8

[a] Calibration of LDR well chamber with NIST seed.
[b] NIST relative combined uncertainty at $k = 2$ for calibration of chamber at M250 and ^{137}Cs beams.

4. Uncertainties in Clinical Dosimetry:
An Example from the Field of Brachytherapy

Prior to 2000, relatively few experimental or computational brachytherapy dosimetry publications using either technique included rigorous uncertainty analyses. Based upon the approaches developed in more recent studies (Gearheart et al. 2000; Nath and Yue 2000; Monroe et al. 2001; Monroe and Williamson 2002; Dolan and Williamson 2006), the 2004 revision of the Task Group 43 (TG-43) protocol (Rivard et al. 2004) now recommended that all publications claiming to provide reference-quality brachytherapy dosimetry data should include an uncertainty analysis adhering to the approach outlined in NIST Technical Note 1297 (Taylor and Kuyatt 1994) (section 1 above). Reference-quality, single-source dose distributions are based upon two independent dosimetry methods: Monte Carlo–based dose estimation and experimental dosimetry, most commonly thermoluminescent detector (TLD) dosimetry in solid phantoms (see chapter 14). Sections 4.1 and 4.2 summarize application of the 2004 TG-43 uncertainty-estimation methodology to Monte Carlo and TLD dosimetry. This will be followed by a brief review of uncertainty estimation for other detector systems (section 4.3) and concludes with a discussion of dosimetric uncertainties in clinical practice (section 4.4).

This chapter [equation (22.5)] defines the problem as one of estimating the combined total uncertainty, $u_C(y)$, where y is the final reported quantity, assuming that $y = f(x_1, x_2,...,x_N)$ for the independent variables x_i for which uncertainties can be estimated. In brachytherapy dosimetry, the quantity y may denote any of the following (as discussed in detail in chapter 14 of this book),

$$y = \begin{cases} \left[\dot{D}_{wat}(r,\theta)/S_K\right]_{MC} = \dfrac{\Delta K_{wat}(r,\theta)}{\Delta S_K} & \text{eq. (14.21)} \\[2ex] \left[\dot{D}_{wat}(r,\theta)/S_K\right]_{meas} = \dfrac{\dot{D}_{wat}(\mathbf{r},t_{ref},Q_{ref},\mathbf{G}_{ref})}{S_K(t_{ref})} & \text{eq. (14.2)} \\[2ex] \Lambda, g_L(r), F(r,\theta), \text{etc.} & \text{Meas or MC} \end{cases} \quad (22.28)$$

For Monte Carlo dose estimates, the x_i may denote, for example, dimensions and compositions of various mechanical seed components or photon cross sections, while mean detector reading, measurement phantom composition, and relative energy response corrections are examples relevant to experimental determinations. To illustrate uncertainty estimation in brachytherapy dosimetry, we summarize the recently published analysis of Dolan and Williamson (2006) for TLD and Monte Carlo dose estimation around the Model 6711 seed.

4.1 Uncertainty of Monte Carlo Dose Estimates in Low-Energy Seed Brachytherapy

One of the first efforts to evaluate the combined uncertainty of Monte Carlo $\left[\dot{D}_{wat}(r,\theta)/S_K \right]_{MC}$ estimates comprehensively was the ^{125}I seed transverse-plane analysis of the updated TG-43 report (Rivard et al. 2004; Williamson and Rivard 2005). In this approach, the relative combined standard uncertainty, $\%u_C(y) = 100u_C(y)/y\%$, for $y = \left[\dot{D}_{wat}(r,\theta)/S_K \right]_{MC}$ is the quadrature sum of four terms:

$$\%u_C(y) = \sqrt{\%u^2(y\,|\,\mu) + \%u^2(y\,|\,\text{geo}) + \%u^2(y\,|\,\text{sp}) + \%u^2(y\,|\,\text{st})}, \quad (22.29)$$

where the first three terms represent propagated uncertainties arising from the Type B uncertainties characteristic of the underlying cross sections and collisional physics model ($\%u(y|\mu)$); the seed geometric model ($\%u(y|\text{geo})$); and the photon spectrum ($\%u(y|\text{sp})$). The Type A statistical uncertainty of the quantity y estimate, inherent to the Monte Carlo technique, is denoted by $\%u(y|\text{st})$. By defining the relative uncertainty propagation factor as

$$\% \frac{\partial f}{\partial x_i} \equiv \frac{x_i}{f} \frac{\partial f}{\partial x_i}, \quad (22.30)$$

equation (22.8) becomes

$$\%u_C(y) = \sqrt{\sum_{i=1}^{N} \left(\% \frac{\partial y}{\partial x_i} \right)^2 \left(\%u(x_i) \right)^2}, \quad (22.31)$$

where $\%u(x_i)$ denotes the relative percent uncertainty of the independent variable x_i with a coverage factor $k = 1$. As written, equation (22.31) ignores correlations.

Dolan et al. (2006) published an extensive study of the impact of uncertainties of the Model 6711 ^{125}I seed geometry on the TG-43 dosimetric ratio, $\dot{D}_{wat}(\vec{r})/S_K$, computed by Monte Carlo simulation. The studied parameters, g_i (and maximum variation, $\pm\left(g_{i,\text{max}} - g_{i,\text{min}} \right)/2$ around their nomimal values, $\bar{g}_i$) included (1) vertical shift of the silver rod (±0.4 mm); (2) horizontal silver rod shift (±0.08 mm); (3) tilting of rod axis relative to capsule axis (±3°); (4) end weld thickness variations (±0.15 mm); (5) radioactive Ag-halide layer thickness variations (1.0 μm to 2.5 μm); (6) uncertainty in Ti capsule radial thickness (±0.01 mm); and (7) manufacturing variations in diameter of the end-face of the beveled rod (60% to 80% of the maximum rod diameter). For each geometric parameter, Monte Carlo simulation was used to calculate $y(g_{i,\text{max}})$ and $y(g_{i,\text{min}})$. By approximating the derivative

[equation (22.30)] with numerical differencing, invoking the rectangular distribution [equation (22.3)], and ignoring correlations, they obtained

$$
\begin{aligned}
\%u(y \mid \text{geo}) &= \sqrt{\sum_{i=1}^{6}\left(\%\frac{\partial y}{\partial g_i}\right)^2 \left(\%u_{g_i}\right)^2} \\
&\approx 100\sqrt{\sum_{i=1}^{6}\left(\frac{\left(y(g_{i,\max})-y(g_{i,\min})\cdot \overline{g}_i\right)}{y(\overline{g}_i)\cdot\left(g_{i,\max}-g_{i,\min}\right)}\right)^2 \left(\frac{g_{i,\max}-g_{i,\min}}{2\sqrt{3}\overline{g}_i}\right)^2} \\
&= 100\sqrt{\sum_{i=1}^{6}\left(\frac{\left(y(g_{i,\max})-y(g_{i,\min})\right)}{2\sqrt{3}\overline{g}_i \cdot y(\overline{g}_i)}\right)^2},
\end{aligned}
\tag{22.32}
$$

where $\overline{g}_i = \left(g_{i,\max}+g_{i,\min}\right)/2$. As table 22-6 shows, geometric uncertainties influence the Model 6711 transverse-axis dosimetric ratio by less than 1%. If we assume that the uncertainties propagated by the seven geometric parameters are maximally correlated ($r(g_i,g_j) = 1$) and use equation (22.19) to estimate $\%u(y|\text{geo})$, we obtain the larger parenthesized values (1.1%, 0.9%, and 0.8%, for the distances 1 cm, 5 cm, and 10 cm) in table 22-6. Dolan et al. (2006) found that the only dose distribution regions to be adversely affected by geometric uncertainties were doses on or near the longitudinal seed axis, where vertical rod positioning uncertainties as large as 7% were noted. The TG-43 uncertainty analysis used a more generous estimate of propagated geometric uncertainty based on studies of seed component mobility (Williamson 2000; Rivard 2001) available at the time. The very small geometric uncertainties referenced in table 22-6 may not be applicable to other seed models and computational dosimetry studies. Each source design is characterized by numerous and unique geometric parameters, most of which have unknown and potentially correlated probability distributions.

Spectral uncertainties were estimated by Dolan et al. (2006) by computing dose distributions for different ^{125}I spectra, namely those recommended by the TG-43 report (Rivard et al. 2004) and the National Nuclear Data Center (NUDAT). Accepting the differences between these two evaluations as representative of spectral uncertainty, the $\%u(y|\text{sp})$ is very small (about 0.5%). Very few data are available to support evaluation of the largest source of Monte Carlo dosimetric uncertainty, namely Type B components arising from uncertainties in the underlying photon cross sections and collisional physics models. Cullen et al. (1997) estimated that the maximum uncertainty in photoionization cross sections in the 5 keV to 100 keV energy range is 2% and argued that in this energy range, the impact of smaller scattering cross-section uncertainties is insignificant. Table 22-7 shows the uncertainty propagation factor $\%\partial\left(\dot{D}_{wat}(r,\pi/2)/S_K\right)_{MC}\Big/\partial\sigma_{PE}$ for three ^{125}I sources as evaluated by numerical differences for Monte Carlo simulations based on two different cross-section libraries (see chapter 14, section 3.2 for more details): DLC-99 (circa 1983) and DLC-146 (1995). These two libraries have total and photoionization linear attenuation coefficient differences of 1.2% and 2.6%, respectively, at

Table 22-6. Uncertainties for Model 6711 ^{125}I Seed Transverse-Axis TLD
and Monte Carlo Dose Estimation
(Adapted from Dolan et al. 2006 with permission from AAPM)

TLD Uncertainties in Measurement of $\dot{D}_{wat}(\vec{r})\,/\,S_K$ for ^{125}I in Solid Water				
Component	**1 cm distance**		**5 cm distance**	
	$\%\sigma_{x_i}$	**Type**	$\%\sigma_{x_i}$	**Type**
Repetitive TLD measurements	1.3%	A	2.2%	A
TLD calibration (including linac calibration)	1.8%	A+B	1.8%	A+B
Absorbed dose energy dependence and PMMA-to-liquid water conversion	0.7%	B	1%	B
Seed and TLD positioning unc. ($\Delta d = 100$ mm)	1.2%	B	0.2%	B
Intrinsic energy-dependence correction	5%	B	5%	B
NIST S_K measurement + one local transfer	1%	B	1%	B
Combined std. uncertainty ($k = 1$)	**5.7%**		**5.9%**	

Uncertainties for Monte Carlo Estimates $\dot{D}_{wat}(\vec{r})\,/\,S_K$ for ^{125}I Model 6711 Seed in Liquid Water			
Distance	**1 cm**	**5 cm**	**10 cm**
Statistics	0.2%	0.3%	0.7%
Photon cross sections	0.7%	2.4%	4.1%
Seed geometry	0.75% (1.1%)*	0.6% (0.9%)*	0.5% (0.8%)*
Source energy spectrum	0.2%	0.3%	0.5%
Combined std. uncertainty ($k = 1$)	**1.1%** **(1.3%)***	**2.5%** **(2.6%)***	**4.2%** **(4.3%)***

*Parenthesized values assume $i,j = 1,\ldots,7$ geometric parameters have correlation coefficients, $r(g_i,g_j) = 1$.

Table 22-7. Relative Uncertainty Propagation Factors
$\left(\%\partial\left(\dot{D}_{wat}(r,\pi/2)\big/S_K\right)_{MC}\big/\partial\sigma_{PE}\right)$ for ^{125}I Seed Brachytherapy

Distance (cm)	Source Model		
	Model 6711[a]	**Bebig Symmetra[b]**	**Point Source[c]**
1 cm	–0.13	–0.31	–0.19
5 cm	–1.42	–1.35	–1.30
10 cm	–2.38	–1.85	–2.38

[a] Unpublished data from Dolan et al. (2006) study.
[b] Hedtjarn et al. (2000). Now marketed as IsoSeed, Model I25.S06.
[c] Author's unpublished data.

28 keV. Assuming that the maximum ±2% uncertainty describes the limits of a uniform probability distribution, $u(\sigma_{PE})$ is 1.2% and using the largest propagation factor for each distance, we obtain $u\left(\dot{D}_{wat}(r,\pi/2)/S_K\right)_{MC} \mid \sigma_{PE}$ values of 0.4%, 1.7%, and 2.9% at distances of 1 cm, 5 cm, and 10 cm, respectively. If we make the very conservative assumption that $u(\sigma_{Coh} + \sigma_{Incoh}) \approx 1.2\%$ for the coherent and incoherent scattering cross sections; assume that the relative uncertainty propagation factors are the same for the scattering and absorption cross sections (most likely a gross overestimate); and note that photoionization constitutes 45% of the total cross section, σ_{tot}, at 28 keV, then $u\left(\dot{D}_{wat}/S_K\right)_{MC} \mid \sigma_{tot} \approx \sqrt{2} \cdot u\left(\dot{D}/S_K\right)_{MC} \mid \sigma_{PE}$. The resultant $k = 1$ propagated uncertainty $\%u\left(\dot{D}_{wat}/S_K\right)_{MC} \mid \sigma_{tot}$ ranges from 0.6% at 1 cm to 4.1% at 10 cm distances. These uncertainties are about half those estimated by Rivard et al. (2004) and Dolan et al. (2006), who interpreted Cullen's 2% estimate, not as maximum uncertainty in photoionization cross sections, but as $\%u\left(\dot{D}_{wat}/S_K\right)_{MC} \mid \sigma_{tot}$ itself.

Table 22-6 indicates that with state-of-the-art codes and cross-section data and painstaking attention to geometric modeling details, relative combined standard uncertainties ($k = 1$) in dose-rate constant evaluation and dose rate at 5 cm of about 1.3% and 2.6%, respectively, can be achieved. These uncertainties are lower than those of the generic TG-43 analysis (2.5% and 5%). Again, we emphasize that each published study must be analyzed individually. For example, a large range of Monte Carlo statistical precisions has been reported, e.g., 0.03% for Rivard's ^{131}Cs study (Rivard 2007) to 3% for Λ estimation (Rivard 2001). Cross-section and photon collision modeling uncertainties appear to dominate the total estimated uncertainty. While these early results are certainly encouraging, more comprehensive studies of uncertainty propagation in transport calculations and quantifying input data uncertainties, especially for radiological data, are badly needed.

4.2 Uncertainty of TLD Dose Measurements in Low-Energy Seed Brachytherapy

Table 22-6 summarizes the uncertainty budget of TLD dosimetry for low-energy brachytherapy for a recent dosimetric characterization of the Model 6711 seed (Dolan et al. 2006). Because equation (14.2) for inferring $\dfrac{\dot{D}_{wat}(\mathbf{r},t_{ref},Q_{ref},\mathbf{G}_{ref})}{S_K(t_{ref})}$ from detector readings consists only of products and quotients of independent input quantities, equation (22.30) can be simplified as $\%\partial\left[\dot{D}_{wat}(\vec{r})/S_K\right]/\partial x_i = 1$. Because Dolan performed as many as 30 readings at some transverse distances, Type A TLD readout precision (expressed as % standard deviation of the mean, i.e., sample standard deviation divided by square root of number of independent observations, per NIST recommendations), is much smaller than the 4% assumed by

previous reviews (Rivard et al. 2004; Williamson and Rivard 2005) and earlier TLD studies (Gearheart et al. 2000; Nath and Yue 2000). Because the seeds used in Dolan's studies had S_K values that were directly traceable to NIST, an S_K uncertainty only slightly larger than the NIST $k = 1$ measurement uncertainty was assumed. Based on the discussion in chapter 14, section 2.2 and AAPM recommendations (Rivard et al. 2004), an uncertainty of 5% was assigned to the intrinsic relative energy dependence, $k_{bq}^{rel}(Q_0 \rightarrow Q_{BTx})$. By comparing Monte Carlo estimates of the absorbed dose energy-response correction, $f^{rel}(Q_0, \mathbf{G}_0 \rightarrow Q_{exp}, \mathbf{G}_{exp}, \mathbf{r})$ [equation (14.10)], and the measurement-phantom correction, $p_{phant,wat}(Q_{exp}, \mathbf{G}_{exp} \rightarrow Q_{ref}, \mathbf{G}_{ref}, \mathbf{r})$ [equation (14.7)], based on the DLC-99 and DLC-146 cross-section libraries, Dolan estimated the uncertainty of these corrections to be on the order of 1% as high-purity polymethylmethacrylate (PMMA) was used as the measurement medium. However, this estimate reflects the fact that the element-to-element cross-section library differences are nearly perfectly correlated, as the main difference between these libraries is the choice of photoionization cross-section normalization. Much larger uncertainties (2% to 6%) (Williamson et al. 1998; Rivard et al. 2004) have been estimated for investigations using RMI Solid Water™ (RMI Gammex, Middleton, WI), assuming that its calcium content by weight is uniformly distributed in the concentration range (1.6% to 2.3%) reported in the literature (see chapter 14). Finally, the uncertainty of the megavoltage beam TLD calibration is based upon Castro et al.'s (2008) detailed uncertainty analysis of the International Atomic Energy Agency (IAEA) TRS-398 protocol [assumed to be applicable to the TG-51 protocol (Almond et al. 1999)], which demonstrated that the $k = 1$ total uncertainty of a photon megavoltage beam absorbed-dose calibration performed with a cylindrical ion chamber is about 1.3%. Combining this with calibration transfer uncertainties of 1% and TLD 0.7%, Type A uncertainty yields a relative combined standard uncertainty of 1.8%.

The final result is that TLD measurements can be used to estimate $\dot{D}_{wat}(\vec{r})/S_K$ with a $k = 1$ uncertainty of about 5.8% under the best possible circumstances. This uncertainty is dominated by the uncertainty associated with estimating TLD-100 energy-dependence corrections. If this uncertainty could be reduced to 2%, (e.g., by replacing TLD with an otherwise equivalent system), measurement uncertainty could be reduced to 3.4%. With more commonly practiced techniques (Solid Water phantoms, fewer TLD readings, ADCL-traceable institutional S_K assays), larger (e.g., 8% to 10%) uncertainties will result (Williamson and Rivard 2005). Using the recommended coverage factor of 2 to specify expanded uncertainty suggests that current brachytherapy dose measurement technologies are not satisfactory, barely achieving 10% measurement accuracy under the best of circumstances, a limit considered to be the maximum acceptable for a quantitative technique (Williamson and Rivard 2005).

4.3 Other Detector Systems and High-Energy Brachytherapy Sources

Of the emerging brachytherapy dose-measurement technologies (see Williamson and Rivard 2005), radiochromic film (RCF) is perhaps the most well-developed alternative to TLD for reference-quality $\dot{D}_{wat}(\vec{r})\,/\,S_K$ measurements. Dempsey et al. (2000) developed a precision dose-measurement system for the relatively insensitive MD-55-2 detector medium [optical density (OD) = 1 for 80 Gy exposure] and demonstrated excellent agreement with Monte Carlo calculations for an HDR ^{192}Ir source. They claimed a 4.6% (k = 2) uncertainty for 0.25 mm pixel pitch including uncertainty components for external beam film calibration and S_K calibration. Their technique included meticulous correction for film non-uniformity [via double-exposure technique (Zhu et al. 1997)], film scanner, and temporal synchronization artifacts. Similar results were found for dosimetry of an LDR ^{137}Cs source by Le et al. (2006), who claimed a k = 1 uncertainty of less than 4% for spatial resolutions of 0.1 mm and doses greater than 5 Gy. Chiu-Tsao et al. (2008) used high-sensitivity film (EBT) to measure relative ^{125}I seed dose distributions and the dose-rate constant using a 6 MV beam to calibrate the film. Based on an extensive analysis, they estimated a 6.9% total uncertainty for their dose-rate constant measurement based upon the single-scanning technique. Monroe et al. (2001) reported uncertainties of 5.7% to 7.4% for MD-55-2 dose-rate measurements around a GliaSite balloon applicator instilled with an organically bound ^{125}I solution with a NIST-traceable activity calibration. In both of these studies, agreement between RCF dose-rate measurements and parallel Monte Carlo calculations was well within experimental uncertainties.

Both the Monroe (Monroe et al. 2001) and Chiu-Tsao (Chiu-Tsao et al. 2008) studies assumed that $k_{bq}^{rel}(Q_0 \rightarrow Q_{BTx}) \approx 1$, i.e., ($M/D_{det}$) was constant, independent of the incident spectrum, Q. A few studies (Chiu-Tsao et al. 2005; Rink et al. 2007) show that $R_{AD}(M,Q) = M(Q)/D_{med}(Q)$ is Q-independent within its 5% to 7% uncertainties. However, almost no studies exist of $k_{bq}^{rel}(Q_0 \rightarrow Q_{BTx})$ corrections derived from relative detector response measurements using rigorous Monte Carlo $(D_{med}/D_{det})(Q)$ estimates. Other phenomena, including dose-rate effect, temporal synchronization, and dose nonlinearity complicate such analyses (Ali et al. 2003, 2005). However, there is no direct evidence that intrinsic energy corrections are needed, and indirect evidence indicates that such corrections are smaller than 5%.

Even fewer analyses of TLD and Monte Carlo uncertainty are available for higher energy sources such as ^{137}Cs and [192]Ir. For a ^{137}Cs tube, Le (Le et al. 2006) performed Monte Carlo calculations for perturbed cross-section libraries, and found that small 1% to 2% assumed uncertainties had negligible impact on computed $\dot{D}_{wat}(\vec{r})\,/\,S_K$ ratios. This is expected, since assuming $D(r) \approx c \cdot e^{-\mu r}/r^2$ implies that $\%u\left(\dot{D}_{wat}/S_K\right)_{MC} \mid \sigma_{tot} \approx \mu r \cdot \%u_\mu$, indicating that higher-energy source cross-section uncertainties are 4- to 6-fold lower than those for ^{125}I sources. Combined with the relative insensitivity of higher-energy dose distributions to

small changes in source construction (Wang and Sloboda 1998), one would expect total uncertainties for Monte Carlo calculations to be quite small, perhaps only slightly larger than the Type A component. One would expect TLD uncertainties to be smaller as well, especially that of the relative energy response correction factor, the dominant ^{125}I uncertainty. However, at least one recent study by Nunn et al. (2008) found a 4% ± 2% difference in (M/D_{det}) for ^{137}Cs compared to 6 MV x-rays and Davis et al. (2003) found 2.0% ± 0.7%.

4.4 Brachytherapy Dosimetry Uncertainties in Clinical Practice

The uncertainties described in sections 4.1 through 4.3 represent the best that can be achieved in a laboratory setting. As discussed above, many published reference-quality dosimetry studies make compromises such as (a) generic energy-response factors, (b) source assays having only secondary or possibly even tertiary traceability to national standards and, (c) use of poorly characterized solid phantom material. Hence the larger ($k = 1$) uncertainties of 4% for dose-rate constants progressing up to 6% for 5 cm dosimetric ratios cited by the TG-43 protocol (Rivard et al. 2004) are probably reasonably realistic estimates of the uncertainty of published TG-43 parameters. Other sources of uncertainty further inflate clinical dose computation uncertainties, including reliance on vendor S_K assays and batch-to-batch random and systematic changes in source construction (impact unknown). Recently, the AAPM formed a task group, TG-138, to document various uncertainties involved in photon-source brachytherapy. A number of publications, namely AAPM TG-40 (Kutcher et al. 1994), TG-56 (Nath et al. 1997), and TG-64 (Yu et al. 1999), have addressed the preliminary uncertainties involved. TG-138 (DeWerd et al. 2009) attempts to address the propagation of the uncertainties in a more comprehensive fashion, including uncertainty propagation from the primary calibration standard through clinical and vendor calibration measurements and the treatment planning system. TG-138 does not address other uncertainties involved in the patient treatment. Table 22-8 shows these uncertainties for the transfer of the primary standard at NIST through the ADCLs to the clinic for the measurement of air-kerma strength (2.54% in table 22-8). The additional contributions to the uncertainty in clinical measurement, treatment-planning systems, etc., add to the uncertainty, resulting in an estimated uncertainty in the clinic for brachytherapy sources to be on the order of 7% before considering the patient.

Numerous other sorts of uncertainties affect clinical assessments of patient dose delivery in brachytherapy. Chief among these are source localization uncertainty, clinical target volume and organ-at-risk boundary-delineation uncertainties (delineation errors), source migration, tissue deformation during treatment, and for low-energy sources, tissue-composition heterogeneities. In contrast to external beam radiotherapy, in which systematic and random geometric uncertainties have been clearly defined and their impact on dose delivery studied (van Herk 2004), relatively little investigation of geometric uncertainties in brachytherapy has been published (Williamson 2005, 2008).

Table 22-8. Propagation of Uncertainties from NIST
through the Measurement of Air-Kerma Strength at the Clinic

Measurement	Quantity (Units)	Relative Uncertainty (%)
NIST WAFAC	Air-kerma strength (AKS)	0.80
ADCL Well chamber	AKS/Amp	0.94
ADCL cal of source	AKS	1.06
ADCL cal of clinic well chamber	AKS/Amp	1.17
Clinic measurement	AKS	1.27
Expanded uncertainty ($k = 2$)	AKS	2.54

Ampere = ?

5. Conclusion

Uncertainty is becoming more of an essential part of understanding in the application of medical physics. The topic of uncertainty propagation should be considered to be an estimate of the quality of the measurement or calculation involved in the treatment. Reduction of uncertainty is always a goal, but it should not be forced at the expense of proper measurement technique and/or patient care. It is important to realize that the uncertainty is an estimate of how close the value is to the conventional true value. The precision of measurement is typically much better than that indicated by the percentages given for the total uncertainty.

Acknowledgment

References

Ali, I., C. Costescu, M. Vicic, J. F. Dempsey, and J. F. Williamson. (2003). "Dependence of radiochromic film optical density post-exposure kinetics on dose and dose fractionation." *Med Phys* 30:1958–1967.
Ali, I., J. F. Williamson, C. Costescu, and J. F. Dempsey. (2005). "Dependence of radiochromic film response kinetics on fractionated doses." *Appl Radiat Isot* 62: 609–617.

Almond, P. R., P. J. Biggs, B. M. Coursey, W. F. Hanson, M. S. Huq, R. Nath, and D. W. O. Rogers. (1999). "AAPM's TG-51 protocol for clinical reference dosimetry of high-energy photon and electron beams." *Med Phys* 26:1847–1870. Also available as AAPM Report No. 67.

Bambynek, M. (2002). "Development of a multi-electrode extrapolation chamber as a prototype of a primary standard for the realization of the quantity of the absorbed dose to water for beta radiation brachytherapy sources." *Nucl Instrum Methods Res A* 492:264–275.

Bohm, T. D., D. W. Pearson, and R. K. Das. (2001). "Measurements and Monte Carlo calculations to determine the absolute detector response of radiochromic film for brachytherapy dosimetry." *Med Phys* 28:142–146.

Castro, P., F. Garcia-Vicente, C. Minguez, A. Floriano, D. Sevillano, L. Perez, and J. J. Torres. (2008). "Study of the uncertainty in the determination of the absorbed dose to water during external beam radiotherapy calibration." *J Appl Clin Med Phys* 9:70–86.

Chiu-Tsao, S. T., Y. Ho, R. Shankar, L. Wang, and L. B. Harrison. (2005). "Energy dependence of response of new high sensitivity radiochromic films for megavoltage and kilovoltage radiation energies." *Med Phys* 32:3350–3354.

Chiu-Tsao, S. T., D. Medich, and J. Munro III. (2008). "The use of new GAFCHROMIC EBT film for ^{125}I seed dosimetry in Solid Water phantom." *Med Phys* 35:3787–3799.

Cullen, D. E., J. H. Hubbell, and L. Kissel. (1997). EPDL97: the Evaluated Photon Data Library, '97 Version. Report No. UCRL—50400, Vol. 6, Rev. 5, University of California, Lawrence Livermore National Laboratory.
http://www.osti.gov/bridge/servlets/purl/295438-uZu33l/webviewable/295438.pdf.

Davis, S. D., C. K. Ross, P. N. Mobit, L. Van der Zwan, W. J. Chase, and K. R. Shortt. (2003). "The response of LiF thermoluminescence dosemeters to photon beams in the energy range from 30 kV x rays to ^{60}Co gamma rays." *Radiat Prot Dosimetry* 106:33–43.

Dempsey, J. F., D. A. Low, S. Mutic, J. Markman, A. S. Kirov, G. H. Nussbaum, and J. F. Williamson. (2000). "Validation of a precision radiochromic film dosimetry system for quantitative two-dimensional imaging of acute exposure dose distributions." *Med Phys* 27:2462–2475.

DeWerd, L. A., M. S. Huq, I. J. Das, G. S. Ibbott, W. F. Hanson, T. W. Slowey, J. F. Williamson, and B. M. Coursey. (2004). "Procedures for establishing and maintaining consistent air-kerma strength standards for low-energy, photon-emitting brachytherapy sources: Recommendations of the Calibration Laboratory Accreditation Subcommittee of the American Association of Physicists in Medicine." *Med Phys* 31:675–681.

DeWerd, L. A., G. S. Ibbott, A. S. Meigooni, M. G. Mitch, M. J. Rivard, K. E. Stump, and B. R. Thomadsen. (2009). "Photon brachytherapy source dosimetric uncertainty analysis: Report of the AAPM Task Group No. 138." *Med Phys* (to be submitted).

Dolan, J., Z. Li, and J. F. Williamson. (2006). "Monte Carlo and experimental dosimetry of an ^{125}I brachytherapy seed." *Med Phys* 33:4675–4684.

Domen, S. R. (1994). "A sealed water calorimeter for measuring absorbed dose." *J Res Natl Inst Stand Technol* 99:121–141.

Gearheart, D. M., A. Drogin, K. Sowards, A. S. Meigooni, and G. S. Ibbott (2000). "Dosimetric characteristics of a new ^{125}I brachytherapy source." *Med Phys* 27:2278–2285.

Giacomo, P. (1981). "News from the BIPM." *Metrologia* 17:69–74.

Goetsch, S. J., F. H. Attix, D. W. Pearson, and B. R. Thomadsen. (1991). "Calibration of ^{192}Ir high-dose-rate afterloading systems." *Med Phys* 18:462–467.

Hedtjarn, H., G. A. Carlsson, and J. F. Williamson. (2000). "Monte Carlo-aided dosimetry of the Symmetra model I25.S06 ^{125}I, interstitial brachytherapy seed." *Med Phys* 27:1076–1085.

International Organization for Standardization (ISO). Guide to the Expression of Uncertainty in Measurement. Geneva, Switzerland: ISO, 1993.

Kutcher, G. J., L. Coia, M. Gillin, W. F. Hanson, S. Leibel, R. J. Morton, J. R. Palta, J. A. Purdy, L. E. Reinstein, G. K. Svensson, M. Weller, and L. Wingfield. (1994). "Comprehensive QA for radiation oncology: Report of AAPM Radiation Therapy Committee Task Group No. 40." *Med Phys* 21:581–618.

Lamperti, P. J., and M. O'Brien. NIST Special Publication 250-58. Calibration of X-ray and Gamma-ray Measuring Instruments. Washington, DC: U. S. Government Printing Office, 2001. http://ts.nist.gov/MeasurementServices/Calibrations/upload/SP250-58.pdf.

Le, Y., I. Ali, J. F. Dempsey, and J. F. Williamson. (2006). "Prospects for quantitative two-dimensional radiochromic film dosimetry for low dose-rate brachytherapy sources." *Med Phys* 33:4622–4634.

Li, Z., R. K. Das, L. A. DeWerd, G. S. Ibbott, A. S. Meigooni, J. Pérez-Calatayud, M. J. Rivard, R. S. Sloboda, and J. F. Williamson. (2007). "Dosimetric prerequisites for routine clinical use of photon emitting brachytherapy sources with average energy higher than 50 keV." *Med Phys* 34:37–40.

Minniti, R., H. Chen-Mayer, S. M. Seltzer, M. S. Huq, L. Bryson, T. Slowey, J. A. Micka, L. A. DeWerd, N. Wells, W. F. Hanson, and G. S. Ibbott. (2006). "The US radiation dosimetry standards for ^{60}Co therapy level beams, and the transfer to the AAPM accredited dosimetry calibration laboratories." *Med Phys* 33:1074–1077.

Minniti R., J. Shobe, S. M. Seltzer, H. Chen-Meyer, and S. Domen. NIST Special Publication 250-74. Absorbed Dose to Water Calibration of Ionization Chambers in a ^{60}Co Gamma-Ray Beam, 2007. http://ts.nist.gov/MeasurementServices/Calibrations/upload/SP250_74.pdf.

Monroe, J. I., and Williamson, J. F. (2002). "Monte Carlo-aided dosimetry of the theragenics TheraSeed model 200 ^{103}Pd interstitial brachytherapy seed." *Med Phys* 29:609–621.

Monroe, J. I., J. F. Dempsey, J. A. Dorton, S. Mutic, J. B. Stubbs, J. Markman, and J. F. Williamson. (2001). "Experimental validation of dose calculation algorithms for the GliaSite RTS, a novel ^{125}I liquid-filled balloon brachytherapy applicator." *Med Phys* 28:73–85.

Nath, R., and N. Yue. (2000). "Dose distribution along the transverse axis of a new 125I source for interstitial brachytherapy." *Med Phys* 27:2536–2540.

Nath, R., L. L. Anderson, J. A. Meli, A. J. Olch, J. A. Stitt, and J. F. Williamson. (1997). "Code of practice for brachytherapy physics: Report of the AAPM Radiation Therapy Committee Task Group No. 56." *Med Phys* 24(10):1557–1598. Also available as AAPM Report No. 59.

Nunn, A. A., S. D. Davis, J. A. Micka, and L. A. DeWerd. (2008). "LiF:Mg,Ti TLD response as a function of photon energy for moderately filtered x-ray spectra in the range of 20-250 kVp relative to ^{60}Co." *Med Phys* 35:1859–1869.

O'Brien, C. M. NIST Quality Manual, Ionizing Radiation Division QM-II, Procedure 3. Calibration of x-ray radiation detectors. Gaithersburg, MD: NIST, 2004. http://physics.nist.gov/Divisions/Div846/QualMan/Procdures/Procedure03v200.pdf.

Rink, A., I. A. Vitkin, and D. A. Jaffray. (2007). "Energy dependence (75 kVp to 18 MV) of radiochromic films assessed using a real-time optical dosimeter." *Med Phys* 34:458–463.

Rivard, M. J. (2001). "Monte Carlo calculations of AAPM Task Group Report No. 43 dosimetry parameters for the MED3631-A/M ^{125}I source." *Med Phys* 28:629-637.

Rivard, M. J. (2007). "Brachytherapy dosimetry parameters calculated for a ^{131}Cs source." *Med Phys* 34:754–762.

Rivard, M. J., B. M. Coursey, L. A. DeWerd, W. F. Hanson, M. S. Huq, G. S. Ibbott, M. G. Mitch, R. Nath, and J. F. Williamson. (2004). "Update of AAPM Task Group No 43 Report: A revised AAPM protocol for brachytherapy dose calculations." *Med Phys* 31:633–674. Also available as AAPM Report No. 84.

Sander, T., and R. F. Nutbrown. NPL Report DQL-RD 004. The NPL Air Kerma Primary Standard TH100C for High Dose Rate ^{192}Ir Brachytherapy Sources. Teddington, UK: NPL, 2006. http://publications.npl.co.uk/npl_web/pdf/dql_rd4.pdf.

Seltzer, S. M., and P. M. Bergstrom. (2003). "Changes in the U.S. primary standards for the air kerma from gamma-ray beams." *J Res Natl Inst Stand Technol* 108:359–381.

Seltzer, S. M., P. J. Lamperti, R. Loevinger, M. G. Mitch, J. T. Weaver, and B. M. Coursey. (2003). "New national air-kerma-strength standards for ^{125}I and ^{103}Pd brachytherapy seeds." *J Res Natl Inst Stand Technol* 108:337–358.

Soares, C. G. NIST Quality Manual, Ionizing Radiation Division QM-II, Procedure 9. Calibration of ophthalmic applicators. Gaithersburg, MD: NIST, 2004. http://physics.nist.gov/Divisions/Div846/QualMan/Procdures/Procedure09v200.pdf.

Stump, K. E., L. A. DeWerd, J. A. Micka, and D. R. Anderson. (2002). "Calibration of new high dose rate ^{192}Ir sources." *Med Phys* 29:1483–1488.

Taylor, B. N., and C. E. Kuyatt. NIST Technical Note 1297. Guidelines for Evaluating and Expressing the Uncertainty of NIST Measurement Results. Washington, DC: U.S. Government Printing Office, 1994. http://physics.nist.gov/Pubs/guidelines/TN1297/tn1297s.pdf.

van der Marel, J. and E. Van Dijk. "Development of a Dutch Primary Standard for Beta Emitting Brachytherapy Sources" in *Standards and Codes of Practice in Medical Radiation Dosimetry,* Proceedings of an International Symposium Standards and Codes of Practice in Medical Radiation Dosimetry. Vienna: IAEA, pp. 93–100, 2003.

van Herk, M. (2004). "Errors and margins in radiotherapy." *Semin Radiat Oncol* 14:52–64.

Wang, R., and R. S. Sloboda. (1998). "Influence of source geometry and materials on the transverse axis dosimetry of ^{192}Ir brachytherapy sources." *Phys Med Biol* 43:37–48.

Williamson, J. F. (2000). "Monte Carlo modeling of the transverse-axis dose distribution of the Model 200 ^{103}Pd interstitial brachytherapy source." *Med Phys* 27:643–654.

Williamson, J. F. "Integration of IMRT and Brachytherapy" in *Image-Guided IMRT.* T. Bortfeld, R. Schmidt-Ullrich, W. DeNeve, and D. E. Wazer (eds.). Heidelberg: Springer-Verlag, pp. 423–438, 2005.

Williamson, J. F. (2008). "Current brachytherapy quality assurance guidance: Does it meet the challenges of emerging image-guided technologies?" *Int J Radiat Oncol Biol Phys* 71:S18–S22.

Williamson, J. F., and M. J. Rivard. "Quantitative Dosimetry Methods for Brachytherapy" in *Brachytherapy Physics: Second Edition.* B. R. Thomadsen, M. J. Rivard, and W. M. Butler (eds.). Madison, WI: Medical Physics Publishing, pp. 233–294, 2005.

Williamson, J. F., B. M. Coursey, L. A. DeWerd, W. F. Hanson, and R. Nath. (1998). "Dosimetric prerequisites for routine clinical use of new low energy photon interstitial brachytherapy sources." *Med Phys* 25:2269–2270.

Yu, Y., L. L. Anderson, Z. Li, D. E. Mellenberg, R. Nath, M. C. Schell, F. M. Waterman, A. Wu, and J. C. Blasko. (1999). "Permanent prostate seed implant brachytherapy: Report of the American Association of Physicists in Medicine Task Group No. 64." *Med Phys* 26(10):2054–2076. Also available as AAPM Report No. 68.

Zhu, Y., A. S. Kirov, V. Mishra, A. S. Meigooni, and J. F. Williamson. (1997). "Quantitative evaluation of radiochromic film response for two-dimensional dosimetry." *Med Phys* 24:223–231.

Problems

1. A medical physicist wants to calibrate a well chamber for assaying air-kerma strength for Model "A" ^{125}I brachytherapy seeds. The clinic has acquired a NIST-calibrated Model "A" seed with a certificate that states S_K = 2.53 U ± 1.62% (k = 2) on 25 September 2008 at 00:00:01 EST. The physicist makes six ionization current (I) measurements at 12:00 EST on 30 September 2008, obtaining the following results: 11.35 pA, 11.43 pA, 11.46 pA, 11.38 pA, 11.37 pA, and 11.42 pA. The uncertainty budget for the well chamber measurements contains a Type B uncertainty of 0.50% (k = 1). Assuming that the half-life of ^{125}I is 59.40 days, calculate the well chamber current, decay corrected to the NIST reference date, including the combined standard uncertainty (k = 1). Determine the well chamber calibration coefficient, S_K / I, and its expanded uncertainty (k = 2).

2. The radial dose function, $g(r)$, for a certain brachytherapy source model may be approximated by a third-order polynomial $g(r) = a_0 + a_1 r + a_2 r^2 + a_3 r^3$, where r is the distance from the source along the transverse axis in centimeters, a_0 = 1.17, a_1 = −1.57×10^{-1} cm^{-1}, a_2 = −8.53×10^{-4} cm^{-2}, a_3 = 5.82×10^{-4} cm^{-3}. The uncertainty in the distance measurement at 2.00 cm is ±0.02 cm. Calculate the value of $g(r)$ at r = 2.00 cm and its uncertainty.

3. A clinic sends one of its ionization chambers to an Accredited Dosimetry Calibration Laboratory (ADCL) for calibration. The calibration certificate reports that the calibration coefficient for that chamber is: N_K = 5.000 × 10^7 Gy/C. The relative combined standard uncertainty expressed as a percentage reported for

   N_K is $\dfrac{u_C(N_K)}{N_K}$ = 1.50%. When the chamber is returned to the clinic, the medical

   physicist uses the chamber to determine the value of the air-kerma rate at a distance of 1 m. The medical physicist measures an ionization current with the chamber of I = 0.10 nA with a standard deviation of $u_A(I)$ = 0.20 pA (Type A uncertainty).
   a. Determine from the measurement the value of the air-kerma rate using equation (22.25) and its uncertainty. Express both the air-kerma rate and the uncertainty in units of mGy/s.
   b. Express the uncertainty of the air-kerma rate obtained in part (a) as a relative uncertainty; i.e., as $\dfrac{u_C(\dot{K})}{\dot{K}}$ both as a fraction and as a percentage.
   c. Determine an interval of air-kerma rates for which one could predict that the measurement would reproduce with a 95% confidence level [HINT: Use equation (22.13)].

d.   A second medical physicist repeats the measurement the next day but instead decides to apply air density and recombination corrections to the measurement of current. The net current is now expressed as $I' = I \cdot K_s \cdot K_{TP}$, where $K_s = 1.005$ is the recombination correction and $K_{TP} = 1.01$ is the air density correction. Assume only Type B uncertainties for these two corrections. For the recombination correction assume an uncertainty of 0.40%. For the air density correction assume the value given in table 22-4 (i.e., the uncertainty budget for the calibration of secondary chambers in terms of air-kerma). Assume the same Type A uncertainty as obtained by the first medical physicist. Build an uncertainty budget for the air-kerma rate similar to table 22-4 but with only four components: the current, the two corrections, and the calibration coefficient. Assume independent variables and use equations (22.26) and (22.27).

e.   Which measurement of the air-kerma rate, between the first and second medical physicists, has a larger uncertainty? Which uncertainty analysis is more accurate and why?

4.   A calibrated ionization chamber having the calibration coefficient of $N_{Dw}^{^{60}Co}$ = 5.000×10^7 Gy/C is immersed in a water tank at 10 cm deep to measure the output of the linear accelerator. The readings are 40.0 nC, 42 nC, 38 nC, 39 nC, 41 nC. The temperature is 22 °C, pressure 750 torr. The barometer manufacturer claims the accuracy of the barometer is within the range of 1% of the reading. The thermometer reads accurate to within 0.5 °C. Develop an uncertainty table for the dose determination in this instance when the calibration coefficient is given an uncertainty of 1.5% at $k = 2$. (Note: ignore the uncertainty in k_Q.)